Available online at www.sciencedirect.com
ScienceDirect
Remote Sensing of Environment 109 (2007) 510–522
Remote Sensing of Environment
www.elsevier.com/locate/rse

Spectral shape-based temporal compositing algorithms for MODIS surface reflectance data

Philip E. Dennison [a,*], Dar A. Roberts [b], Seth H. Peterson [b]

[a] Center for Natural and Technological Hazards, Department of Geography, University of Utah, Salt Lake City, UT 84112, USA
[b] Department of Geography, University of California, Santa Barbara, CA 93106, USA

Received 18 July 2006; received in revised form 3 December 2006; accepted 3 February 2007

Abstract

Spectral similarity metrics have previously been used to select representative spectra from a class for use in spectral mixture modeling. Since the tasks of spectral selection for spectral mixture modeling and spectral selection for temporal compositing are similar, these metrics may have utility for temporal compositing. This paper explores the use of two spectral similarity metrics, endmember average root mean square error (EAR) and minimum average spectral angle (MASA), for constructing temporal composites. EAR and MASA compositing algorithms were compared against four previously used algorithms, including maximum NDVI, minimum view zenith angle, minimum blue, and median red. A total of 10 different algorithms were used to create 16-day composites of Moderate Resolution Imaging Spectroradiometer (MODIS) surface reflectance data over a 6-year period. Algorithm performance was assessed based on short-term temporal variability in spectral reflectance and in a selection of indices, both within a southwestern California study area and within five land-cover class subsets. EAR compositing produced the lowest variability for 4 out of 7 MODIS bands, as measured by the root mean square of time series residuals. MASA or EAR compositing produced the lowest root mean square residual values for all of the tested indices. To assess how compositing algorithms might affect remote sensing correlations with biophysical variables, correlations between indices calculated from different composites and live fuel moisture were compared. Correlations between indices and live fuel moisture were higher for shape-based composites compared with the standard composites.
© 2007 Elsevier Inc. All rights reserved.

Keywords: Temporal compositing; Spectral matching; Endmember selection; MODIS; Live fuel moisture

1. Introduction

Temporal compositing has routinely been applied to remote sensing time series data as a means of minimizing the impacts of cloud effects and changing view geometry, and as a form of data compression (Qi & Kerr, 1997). Temporal compositing examines the values of a band or index within a pixel across time and, using an algorithm, selects the single best band or index value to represent the entire time period. The resulting composite image can then be compared with other composites to characterize vegetation phenology and productivity, classify land cover, and detect change over time (Box et al., 1989; Churkina et al., 2005; Duchemin et al., 1999; Friedl et al., 2002; Loveland et al., 2000; Lunetta et al., 2006; Paruelo & Lauenroth, 1998). The challenge of compositing as described by Qi and Kerr (1997) is retaining useful information in the composited data while at the same time suppressing background "noise" caused by cloud, atmospheric, or BRDF effects. Choice of compositing algorithms can impact the variability of the composited data and of indices calculated from the composited data (Roy, 1997) and the accuracy of classifications for specific applications (Chuvieco et al., 2005).

A multitude of temporal compositing algorithms have been developed for moderate-to-coarse resolution remote sensing systems. Holben (1986) established the use of the maximum value of a vegetation index for compositing. Maximum value compositing has been the most commonly used compositing algorithm, but it has been found to favor forward-scattering

* Corresponding author. Tel.: +1 801 585 1805; fax: +1 801 581 8219.
E-mail address: dennison@geog.utah.edu (P.E. Dennison).

0034-4257/$ - see front matter © 2007 Elsevier Inc. All rights reserved.
doi:10.1016/j.rse.2007.02.009

view geometries and is susceptible to atmospheric contamination (Cihlar et al., 1997; Kasischke & French, 1997; van Leeuwen et al., 1999). Several other methods rely on low reflectance in the visible wavelengths to discriminate clear pixels from cloud-contaminated pixels. Examples of this type of algorithm include selecting the minimum blue band value (Vermote & Vermeulen, 1999), the minimum red band value (Cabral et al., 2003; Chuvieco et al., 2005), or the median red band value (Dennison et al., 2005). Relying on minimum reflectance may favor selection of shadowed pixels, as occurs for the minimum blue compositing method (Roy et al., 2002). A third class of algorithms takes into account view geometries, either by explicitly correcting for bidirectional reflectance distribution function (BRDF) (van Leeuwen et al., 1999; Schaaf et al., 2002) or by selecting the minimum view zenith angle (Chuvieco et al., 2005). Selecting for minimum view zenith angle also minimizes the observational area of pixels by favoring view zeniths closer to nadir, but minimum view zenith selection requires rigorous prescreening of data for cloud effects. BRDF modeling accounts for both view and solar zeniths and azimuths. An observationally-based BRDF model is used to correct MODIS data to nadir reflectance for the MOD43B4 16-day Nadir BRDF-Adjusted Reflectance product (Schaaf et al., 2002). A fourth class of algorithms uses thermal infrared measures for compositing, such as thresholding brightness temperature (Gutman et al., 1994) or maximum surface temperature (Cihlar et al., 1994; Roy, 1997). Algorithms can also combine multiple criteria, including view zenith angles, minimum band brightness or maximum index values, and brightness temperatures (Cabral et al., 2003; Carreiras & Pereira, 2005; Carreiras et al., 2003; Cihlar et al., 1994).

This study introduces a new class of compositing algorithms based on two measures of spectral similarity, endmember average root mean square error (EAR) and minimum average spectral angle (MASA). This research conclusively demonstrates that these novel algorithms are able to reduce short-term variability in spectral indices across several land cover types within a limited study area.

2. Background

2.1. Spectral matching algorithms

Spectral matching algorithms are used to determine similarity between reference spectra and image spectra. These algorithms use a similarity metric to resolve the identity or composition of an unknown spectrum (e.g. Boardman et al., 1995; Clark & Roush, 1984; Dennison et al., 2004; Harsanyi & Chang, 1994; Kruse et al., 1993). Two spectral matching algorithms have been widely used for determining spectral similarity: multiple endmember spectral mixture analysis (MESMA; Roberts et al., 1998) and spectral angle mapper (SAM; Kruse et al., 1993). MESMA is based on linear spectral mixture modeling (Adams et al., 1993), and models a spectrum as the linear combination of spectral "endmembers". Each endmember is multiplied by a fractional abundance, such that the reflectance of a modeled spectrum ($\rho'\lambda$) is determined by the sum of the reflectance of each material within a pixel multiplied by its fractional cover:

$$\rho'_\lambda = \sum_{i=1}^{N} f_i * \rho_{i\lambda} + \varepsilon_\lambda \quad (1)$$

where $\rho_{i\lambda}$ is the reflectance of endmember i for a specific band (λ), f_i is the fraction of the endmember, N is the number of endmembers, and ε_λ is a residual term. Linear spectral mixing models typically use a dark "shade" endmember that controls for brightness, along with one or more non-shade endmembers. MESMA extends linear spectral mixture modeling by allowing the number and identity of non-shade endmembers to vary on a per-pixel basis. MESMA measures spectral similarity by the root mean square of the residual term:

$$\mathrm{RMSE} = \sqrt{\frac{\sum_{\lambda=1}^{M} (\varepsilon_\lambda)^2}{M}} \quad (2)$$

where M is the number of bands (Roberts et al., 1998).

SAM measures spectral similarity using the angle between two spectral vectors. The length of a spectrum vector (L_ρ) is calculated as:

$$L_\rho = \sqrt{\sum_{\lambda=1}^{M} \rho_\lambda^2} \quad (3)$$

and spectral angle (θ) is calculated as:

$$\theta = \cos^{-1}\left(\frac{\sum_{\lambda=1}^{M} \rho_\lambda \rho'_\lambda}{L_\rho L_{\rho'}}\right) \quad (4)$$

where L_ρ is the length of the endmember vector and $L_{\rho'}$ is the length of the modeled spectrum vector calculated using Eq. (3). Since the angle between vectors is independent of vector length, spectral angle does not vary with the brightness of the two spectra being compared.

MESMA and SAM can both be used to measure the spectral similarity within a class of spectra. This class normally consists of spectra of a single land cover type or vegetation species (Ballantine et al., 2005; Dennison & Roberts, 2003a,b; Powell et al., 2007). An example of a class consisting of five spectra, numbered 1 through 5, is shown in Fig. 1. Each spectrum within the class is a candidate endmember for modeling the other spectra in the class using MESMA or SAM. Fig. 1 shows each spectrum in the class being used as an endmember to model every other spectrum in the class. A spectral matching algorithm can be used to measure spectral similarity between each pairing of an endmember and a modeled spectrum. In Fig. 1, the spectral similarity metric is represented with the symbol $\sigma_{i,j}$, where i is the endmember number and j is the modeled spectrum number. For MESMA, $\sigma_{i,j}$ is RMSE while for SAM $\sigma_{i,j}$ is θ, the spectral angle. Dennison et al. (2004) showed that

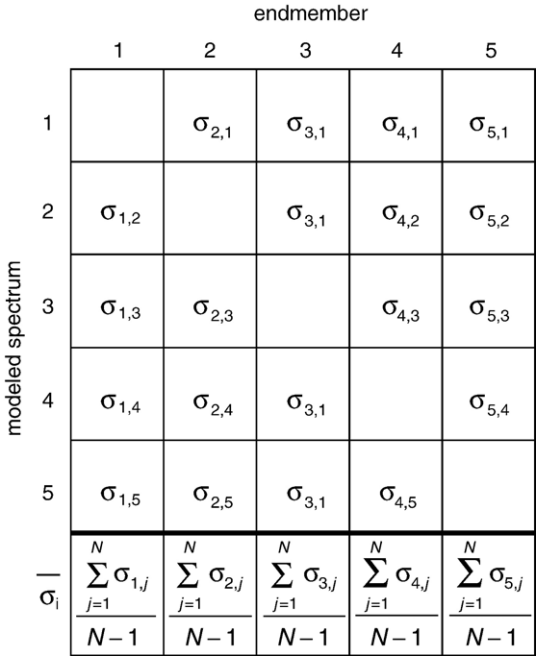

Fig. 1. A matrix showing a class of five spectra (endmembers) being used to model each spectrum in the class, producing an error metric for each model ($\sigma_{i,j}$) and an average error metric for each endmember spectrum ($\bar{\sigma}_i$).

for each endmember, an average spectral similarity metric, $\bar{\sigma}_i$, can be calculated:

$$\bar{\sigma}_i = \frac{\sum_{j=1}^{N} \sigma_{i,j}}{N-1} \tag{5}$$

where i is endmember, j is the modeled spectrum, and N is the number of endmembers. The endmember with the lowest average spectral similarity metric is the endmember that, on average, best models its spectral class. Dennison and Roberts (2003a) refer to this endmember as being the most "representative" of its class.

Dennison and Roberts (2003a) examined the similarity of spectra belonging to the same vegetation species using MESMA. Airborne Visible Infrared Imaging Spectrometer (AVIRIS) spectra were extracted from polygons containing field-verified species composition and classed by species. Endmember average RMSE (EAR) was calculated for each spectrum to determine which spectrum in each class best modeled the class:

$$\mathrm{EAR}_i = \frac{\sum_{j=1}^{N} \mathrm{RMSE}_{i,j}}{N-1} \tag{6}$$

The spectrum with the minimum EAR value indicated the spectrum that had the best average fit to the other spectra within its class, in terms of RMSE. Dennison and Roberts (2003a) used the minimum EAR endmember for multiple vegetation species classes to map species across the entire image. Minimum EAR values were also compared between species classes to indicate the relative amount of spectral diversity within each class. Dennison and Roberts (2003b) introduced a constraint to EAR to prevent low reflectance spectra from being selected. The fraction of the non-shade endmember was limited to a maximum value, which increased the RMSE for darker spectra. Dennison and Roberts (2003b) also demonstrated that phenological changes were expressed in minimum EAR endmembers extracted from a time series of AVIRIS data. Ballantine et al. (2005) used EAR to select representative endmembers from a library of MODIS image and reference spectra for mapping landforms across North Africa, and Powell et al. (2007) used EAR to select endmembers suitable for mapping impervious surfaces in the Brazilian Amazon.

Dennison et al. (2004) introduced minimum average spectra angle (MASA). MASA is the spectral angle equivalent to EAR, with θ replacing RMSE as the error metric:

$$\mathrm{MASA}_i = \frac{\sum_{j=1}^{N} \theta_{i,j}}{N-1} \tag{7}$$

The spectrum with the minimum MASA value is the spectrum that has the best average fit to the other spectra within its class, in terms of spectral angle. Unlike EAR, MASA is only sensitive to differences in spectral shape and is not sensitive to differences in brightness. EAR and MASA are not equivalent, but are closely related for spectral classes that have small variations in albedo (Dennison et al., 2004). If EAR is unconstrained, the same spectrum frequently possesses the minimum EAR and MASA values within a class.

While EAR and MASA have predominantly been used to select spectra from classes extracted from a single land cover type or vegetation species, there are no explicit limitations on the membership of the spectral classes used to calculate EAR and MASA. A spectral class could be comprised of spectra from the same location, measured at different times. In this case, EAR or MASA would select the single spectrum that has the best average fit to the spectra collected over a period of time. Thus, EAR and MASA have potential for use in temporal compositing algorithms. Unlike existing compositing algorithms, these EAR and MASA-based algorithms can select composite spectra based on how well they match the shape of the spectra within the compositing period. Spectra with transient cloud or atmospheric contamination, or infrequent BRDF effects, are unlikely to be selected because they poorly match the shape of other spectra within the compositing period.

2.2. Using temporal composites to monitor live fuel moisture

To demonstrate that choice of compositing algorithm might affect apparent relationships between remote sensing data and a biophysical variable, correlations between MODIS spectral indices and live fuel moisture were compared for different compositing algorithms. Several previous studies have examined correlations between MODIS spectral indices and live fuel moisture of chaparral vegetation (Dennison et al., 2005; Roberts et al., 2006;

Stow et al., 2005). Live fuel moisture is calculated as the mass of water as a percentage of the dry mass of vegetation (m_d):

$$\text{live fuel moisture} = \frac{m_w - m_d}{m_d} \quad (8)$$

where m_w is the mass of the undried vegetation. These previous studies have compared chaparral live fuel moisture to two classes of indices: greenness and moisture indices. Greenness indices utilize the strong spectral contrast between higher NIR or green reflectance and lower red reflectance caused by chlorophyll absorption, while moisture indices rely on water absorption features in the short-wave infrared.

Previous studies have disagreed as to whether specific greenness indices or moisture indices are more strongly related to live fuel moisture. Dennison et al. (2005) used a median red compositing algorithm to create 16-day MODIS surface reflectance composites. These composites were used to calculate normalized difference vegetation index (NDVI; Rouse et al., 1973) and normalized different water index (NDWI; Gao, 1996). Correlations between these two indices and live fuel moisture were examined, and NDWI was found to have a stronger relationship with live fuel moisture than NDVI. Stow et al. (2005) used the MODIS 8-day surface reflectance product to generate a monthly time series of MODIS index values. They compared live fuel moisture values to NDWI and visible atmospherically resistant index (VARI; Gitelson et al., 2002) values, and found that VARI was more strongly correlated with live fuel moisture. Roberts et al. (2006) examined the relationships between live fuel moisture and a larger suite of vegetation indices. They used an EAR compositing algorithm similar to the one presented in this paper to calculate 16-day MODIS composites, which were then used to derive NDVI, NDWI, VARI, the vegetation index green (VIg; Gitelson et al., 2002), the enhanced vegetation index (EVI; Huete et al., 2002), and normalized difference indices using MODIS bands 6 and 7 (NDII6 and NDII 7; Hunt & Rock, 1989). Roberts et al. (2006) found consistently stronger relationships with live fuel moisture for visible-based greenness indices (VARI and VIg) than for moisture indices.

3. Methods

3.1. Data

Ten compositing algorithms were compared for an approximately 330 by 190 km study area covering southern California, USA (Fig. 2). The study area was selected based on its diversity of land cover, including urban and agricultural land uses, and shrubland and desert vegetation cover. The study area was also selected to include long-term chaparral live fuel moisture monitoring sites with Los Angeles County, California (Fig. 2).

The MODIS Terra level 2 g global half kilometer daily surface reflectance product (MOD09GHK) was used as the primary input for the compositing algorithms. See Vermote et al. (1997) and Vermote et al. (2002) for a description of MODIS surface reflectance processing. MOD09GHK includes 7 visible, near infrared, and shortwave infrared bands (469 nm, 555 nm, 645 nm, 857 nm, 1240 nm, 1640 nm, and 2130 nm), has a sinusoidal projection, and a ground sample distance of approximately 460 m. MOD09GHK data for 2053 days, spanning 24 February 2000 to 31 December 2005, were used to construct 16-day composites for the study area. The 16-day composite period was selected to match the orbital cycle of the Terra satellite, current standard MODIS vegetation index products, and several other MODIS land products.

All daily surface reflectance data were screened for cloud effects and view zenith angle. The MODIS Terra level 2 g 1 km surface reflectance quality product (MOD09GST) was used to create a cloud mask. MOD09GST contains cloud masks derived from the MODIS MOD35 cloud mask product. Flags for cloud cover, cloud shadow, and cirrus were used to create a cloud effects mask, which was then resampled to match the resolution of the MOD09GHK product. The MODIS Terra level 2 g 1 km daily geolocation angles product (MODMGGAD) was used to screen out high view zenith angles. View zenith angles higher than 45° were masked out and then resampled to match the resolution of the MOD09GHK product. The resulting masks were applied to the daily surface reflectance data. All unmasked pixels were required to have no cloud cover, and no cloud shadow, and no cirrus, and a view zenith angle of 45° or less, as indicated by the MOD09GST and MODMGGAD data flags.

The remaining dates for each pixel within a 16-day period formed a spectral class, and were composited using 10 different algorithms (Table 1). Each algorithm selected a spectrum from the 16-day period for each pixel in the study area. The algorithms were used to generate a time series of 129 sixteen-day composites spanning 2000–2005.

3.2. Compositing algorithms

Four algorithms previously utilized for compositing MODIS data were used to calculate baseline composite time series. A

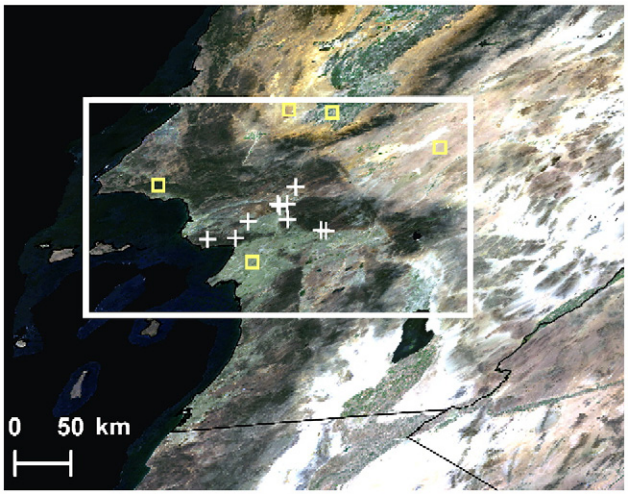

Fig. 2. A sinusoidally projected MODIS "true color" composite (bands 1, 4, 3) of southern California. The study area is outlined by the large rectangle. The small squares outline 10 km by 10 km areas with uniform land cover used for residual analysis. The locations of 11 live fuel moisture samples sites are marked by white crosses.

Table 1
Descriptions of the compositing algorithms used to construct 16-day temporal composites of daily MODIS surface reflectance data

Composite abbreviation	Description	Reference
maxNDVI	Selects spectrum with maximum normalized difference vegetation index (NDVI).	Holben (1986)
minVZA	Selects spectrum with minimum view zenith angle (VZA).	Chuvieco et al. (2005)
minblue	Selects spectrum with minimum band 3 (469 nm) reflectance.	Vermote and Vermeulen (1999)
medred	Selects spectrum with median band 1 (645 nm) reflectance.	Dennison et al. (2005)
EAR10 EAR20 EAR30 EAR40 EAR50	Selects spectrum with minimum endmember average RMSE (EAR). Maximum mean shade fraction constrains the brightness of the selected spectrum and has a value of 10%, 20%, 30%, 40%, or 50%.	Dennison and Roberts (2003a)
MASA	Selects spectrum with minimum average spectral angle (MASA).	Dennison et al. (2004)

maximum value composite (Holben, 1986) using NDVI (maxNDVI) was used to select the spectrum with the maximum normalized difference ratio of bands 1 (645 nm) and 2 (856 nm) within the 16-day composite period for each pixel. A minimum view zenith angle (minVZA) composite was used to select the spectrum with the minimum sensor view zenith angle (Chuvieco et al., 2005). A minimum blue (minblue) algorithm developed by Vermote and Vermeulen (1999) was used to select the spectrum containing the minimum band 3 (469 nm) reflectance, and a median red (medred) algorithm used by Dennison et al. (2005) was used to select the spectrum containing the median band 1 reflectance.

The four baseline compositing algorithms were compared with five algorithms based on EAR and one algorithm based on MASA. For the shape-based compositing algorithms, the number of unmasked dates within the compositing period was determined for each pixel. Since both EAR and MASA require at least three spectra within a spectral class to find the single spectrum with the best average fit, the spectrum with the lower red reflectance was selected when only two spectra were available within a 16-day compositing period. For three or more unmasked spectra within a pixel for a compositing period, all spectra were placed within the same spectral class and EAR and MASA were calculated for each spectrum. The spectrum with the lowest EAR or MASA value was selected as the composite spectrum for that pixel.

The shape-based compositing algorithms differed by the constraints that were placed on endmember selection. For the MASA compositing algorithm, no constraints were placed on endmember selection and the composite spectra were selected entirely based on spectral shape. Five variations of an EAR compositing algorithm were compared. Unlike MASA, EAR can be constrained to select endmembers based both on brightness and spectral shape. All five EAR algorithms used a maximum non-shade endmember fractional constraint of 100%, which penalizes low reflectance endmembers by increasing their EAR value (Dennison & Roberts, 2003b).

A new constraint on the shade fraction was used to penalize high reflectance endmembers as well. The mean shade fraction was calculated for each endmember, and only endmembers with mean shade fractions below a specified threshold could be selected for the composite. To illustrate how the mean shade fraction and RMS were used for compositing, an example using three spectra derived from the composite period spanning days 241–256 in 2005 is shown in Fig. 3. Spectrum “a” has the lowest EAR value, but since it is the brightest spectrum in the compositing period it also has the highest mean shade fraction (14%). A maximum mean shade fraction constraint limits the mean shade fraction of the selected spectrum to a value below a fixed threshold. In this example, if the maximum mean shade fraction constraint was greater than 14%, then spectrum “a” would be selected because it had the lowest EAR value and a mean shade fraction below the constraint. If the maximum mean shade fraction constraint was set at 10%, then spectrum “b” would be selected because it has the lowest EAR value with a mean shade fraction below the constraint.

Five different maximum mean shade fraction constraints were tested. Higher constraints allow spectral selection to be based more on spectral shape and less on relative brightness, while lower, more stringent constraints allow spectral selection to be based more on relative brightness and less on spectral shape. The five maximum mean shade fraction constraints tested were 10%, 20%, 30%, 40%, and 50%. The EAR algorithms will be referred to as EAR10, EAR20, EAR30, EAR40, and EAR50, with the number corresponding to the maximum mean shade fraction constraint.

3.3. Variability analysis

The short-term temporal variability of the composite times series was assessed for each of the 10 compositing algorithms.

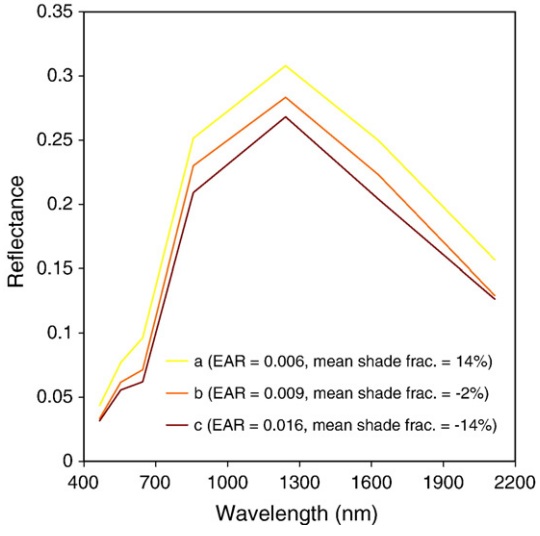

Fig. 3. Three MODIS spectra for the Clark Motorway live fuel moisture site corresponding to days 242 (a), 251 (b), and 249 (c) of 2005.

Table 2
Spectral indices calculated for each of the 16-day MODIS composites listed in Table 1

Index	Formula (band center wavelengths in nm)	Reference
VIg	$\frac{\rho_{555}-\rho_{645}}{\rho_{555}+\rho_{645}}$	Gitelson et al. (2002)
VARI	$\frac{\rho_{555}-\rho_{645}}{\rho_{555}+\rho_{645}-\rho_{469}}$	Gitelson et al. (2002)
NDVI	$\frac{\rho_{857}-\rho_{645}}{\rho_{857}+\rho_{645}}$	Rouse et al. (1973)
EVI	$2.5\times\frac{\rho_{857}-\rho_{645}}{\rho_{857}+6\times\rho_{645}-7.5\times\rho_{469}+1}$	Huete et al. (2002)
NDWI	$\frac{\rho_{857}-\rho_{1240}}{\rho_{857}+\rho_{1240}}$	Gao (1996)
NDII6	$\frac{\rho_{857}-\rho_{1640}}{\rho_{857}+\rho_{1640}}$	Hunt and Rock (1989)
NDII7	$\frac{\rho_{857}-\rho_{2130}}{\rho_{857}+\rho_{2130}}$	Hunt and Rock (1989)

Large deviations in one composite's reflectance or index values from a longer-term trend may indicate suboptimal selection of spectra by the compositing algorithm. These deviations can be caused by cloud effects such as unmasked cloud or cloud shadow contamination, or by BRDF, although sudden phenological or land cover change may also produce similar deviations. Short-term variability within a five composite (80 days) moving window was examined for seven MODIS bands and for seven commonly used vegetation indices listed in Table 2. For each band or index, variability was measured using a filtering technique described by Roberts et al. (2006). A low pass filter was applied to a moving window of five composites, and a residual was calculated as the raw value from the central composite minus the filtered value from the central composite. Residuals were not calculated for the first two composites, the last two composites, or for any missing values in the composite time series. Composite residuals can be compared within bands or indices, but should not be directly compared between different bands or indices. Fig. 4 compares time series of NDWI values for two compositing algorithms, maxNDVI and MASA. Fig. 5 shows the residuals for the filtered time series, along with the root mean square of the residuals for each series. In this example, MASA has lower variability than maxNDVI, as shown by the smaller residuals and lower root mean square residual value.

Root mean square residuals were calculated for each pixel, for each band or index, and for each composite produced by a different compositing algorithm. To permit comparison of compositing algorithms over the entire study area and within specific land cover types, root mean square residuals were spatially averaged. To calculate the average root mean square residual for the entire study area, water areas within the study area were masked and the mean root mean square residual was calculated for all remaining pixels. To examine how land cover impacts residuals, root mean square residuals were averaged within five 10 km by 10 km sites containing uniform land cover. The locations of land cover analysis sites containing agricultural, chaparral, desert, grassland, and urban land cover types are shown in Fig. 2.

3.4. Live fuel moisture analysis

Higher variability in indices caused by cloud contamination or BRDF effects may reduce the strength of correlations between indices and biophysical variables. Correlations between index

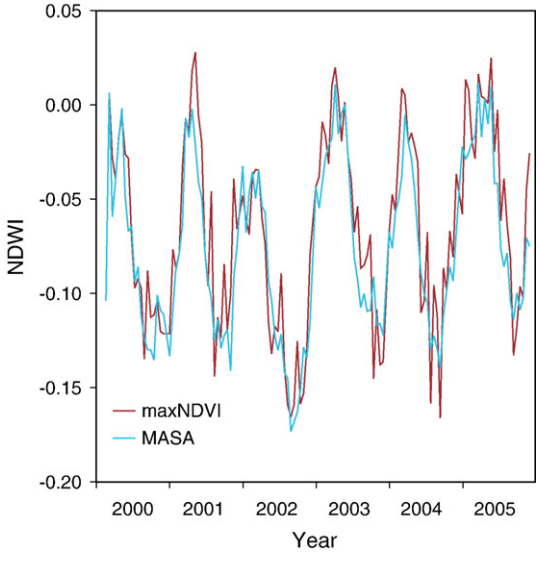

Fig. 4. NDWI values for the Clark Motorway live fuel moisture sampling site, calculated from the maxNDVI and MASA 16-day composites.

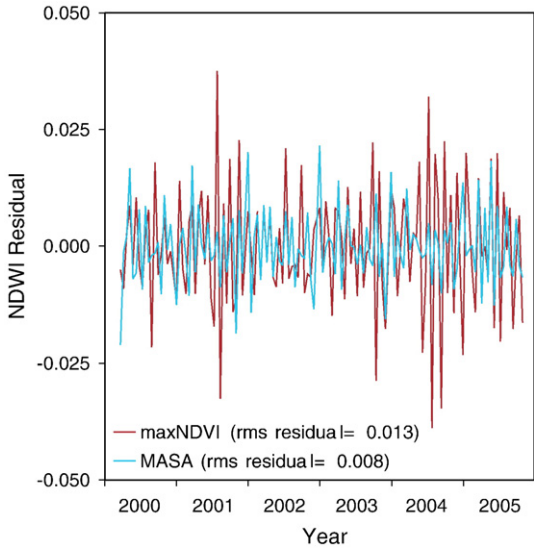

Fig. 5. NDWI residuals for the Clark Motorway live fuel moisture sampling site, calculated from NDWI values shown in Fig. 4.

values and live fuel moisture were examined for the 10 compositing algorithms. Live fuel moisture was sampled at 14 sites in Los Angeles County, California, USA by the Los Angeles County Fire Department. Sampling occurred approximately once every 3 weeks during the 2000–2005 study period (LACFD, 2000–2005). One to three species were sampled at each site using methods described by Countryman and Dean (1979) and Weise et al. (1998). Three sites were eliminated from the analysis due to high land cover heterogeneity within the MODIS pixel containing the sample site or due to a fire in close proximity to the site during the study period (Roberts et al., 2006).

Linear regression was used to assess the relationship between index values and 16 live fuel moisture samples at 11 sites. r^2 values were calculated for each sample, and the average r^2 values for all samples were compared by index and by composite. A significance test outlined by Dennison et al. (2005) was used to determine the number of samples that possessed significantly lower or higher correlations for each composite, compared with the best composite. Correlation coefficients were transformed to a normalized distribution using a Fisher z-transform (Papoulis, 1990):

$$z_f = 0.5 \cdot \ln\left(\frac{1+r}{1-r}\right) \quad (9)$$

where r is Pearson's correlation coefficient. The difference in individual z_f scores was then calculated as:

$$z = \frac{z_{f1} - z_{f2}}{\sqrt{\frac{1}{n_1 - 3} + \frac{1}{n_2 - 3}}} \quad (10)$$

where n is the number of samples (Papoulis, 1990). A one-tailed test was used to determine whether z was significantly positive or negative to indicate a significantly stronger or weaker correlation.

4. Results

Dennison and Roberts (2003a) showed that the minimum EAR value is an indicator of the heterogeneity within a spectral class. Similarly, EAR and MASA values calculated by the shaped-based compositing algorithms are indicators of the temporal spectral heterogeneity within a 16-day composite period. Fig. 6 shows the mean minimum EAR values for all EAR30 composites in the time series. EAR values are high along the edges between two land cover types, for example, between land and water. Agricultural areas such as the Central Valley (Fig. 6 top center–right), the Santa Maria Valley (top left) and Imperial Valley (bottom right) also exhibit high EAR values. EAR values are high in these cases because of view zenith effects on the spatial resolution of MODIS data. As view zenith increases, the effective observational area of each MODIS pixel also increases (Wolfe et al., 1998). Changes in the observational area will most strongly impact heterogeneous (e.g. patchwork fields) or discontinuous (e.g. shorelines) land cover. As different fractions of multiple land cover types are measured within the observational area of a pixel, the spectral response of that pixel will vary. The dynamic nature of agricultural areas also contributes to their higher EAR values. Elevated EAR values show evidence of increased spectral variability at higher elevations in the San Gabriel and San Jacinto mountain ranges. Rapid changes in snow cover at higher elevations can create radically different spectral response over short periods of time. High EAR values at high elevation reflect snow deposition and ablation on relatively short time scales.

Tables 3 and 4 summarize the study area root mean square residuals for image band and index values. The EAR composites

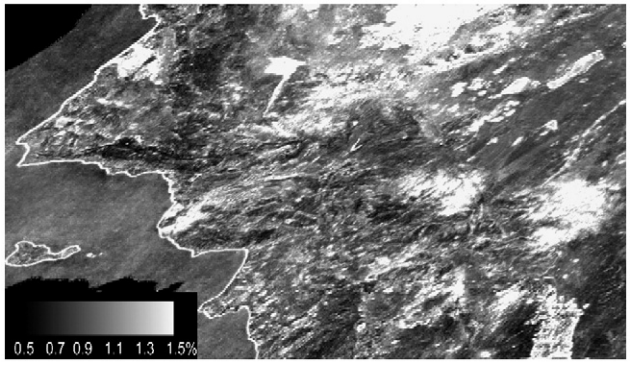

Fig. 6. Mean minimum EAR (for all composites in the time series) for the spectra selected by the EAR30 compositing algorithm.

Table 3
The mean of study area root mean square residuals for MODIS reflectance bands, shown as percent reflectance

Composite	MODIS band						
	Band 1	Band 2	Band 3	Band 4	Band 5	Band 6	Band 7
MASA	1.20%	2.31%	0.68%	1.03%	2.51%	2.25%	1.70%
EAR50	0.97%	1.56%	0.71%	0.85%	1.56%	1.43%	1.19%
EAR40	0.93%	1.55%	0.65%	0.81%	1.56%	1.44%	1.18%
EAR30	0.89%	1.53%	0.61%	0.77%	1.55%	1.44%	1.18%
EAR20	0.85%	1.46%	0.57%	0.73%	1.49%	1.39%	1.15%
EAR10	0.82%	*1.42%*	0.57%	0.72%	*1.44%*	*1.32%*	*1.13%*
maxNDVI	1.23%	2.56%	0.71%	1.08%	2.69%	2.22%	1.75%
medred	*0.72%*	1.83%	0.55%	*0.66%*	1.95%	1.46%	1.21%
minblue	0.84%	1.68%	*0.50%*	0.70%	1.77%	1.48%	1.32%
minVZA	1.24%	1.65%	1.02%	1.14%	1.82%	1.49%	1.37%

Minimum values for each band are shown in italics.

Table 4
The mean of study area root mean square residuals for seven spectral indices

Composite	Index						
	VIg	VARI	NDVI	EVI	NDWI	NDII6	NDII7
MASA	*0.0098*	0.0161	*0.0170*	0.0178	*0.0100*	*0.0162*	*0.0211*
EAR50	0.0105	*0.0160*	0.0201	0.0156	0.0113	0.0193	0.0248
EAR40	0.0105	0.0163	0.0199	0.0156	0.0111	0.0191	0.0247
EAR30	0.0105	0.0166	0.0199	*0.0155*	0.0112	0.0189	0.0248
EAR20	0.0107	0.0173	0.0206	0.0155	0.0117	0.0195	0.0260
EAR10	0.0116	0.0189	0.0231	0.0162	0.0133	0.0217	0.0296
maxNDVI	0.0161	0.0317	0.0234	0.0264	0.0153	0.0236	0.0312
medred	0.0125	0.0200	0.0249	0.0220	0.0180	0.0254	0.0348
minblue	0.0164	0.0313	0.0277	0.0187	0.0167	0.0250	0.0346
minVZA	0.0123	0.0208	0.0259	0.0158	0.0217	0.0267	0.0347

Minimum values for each index are shown in italics.

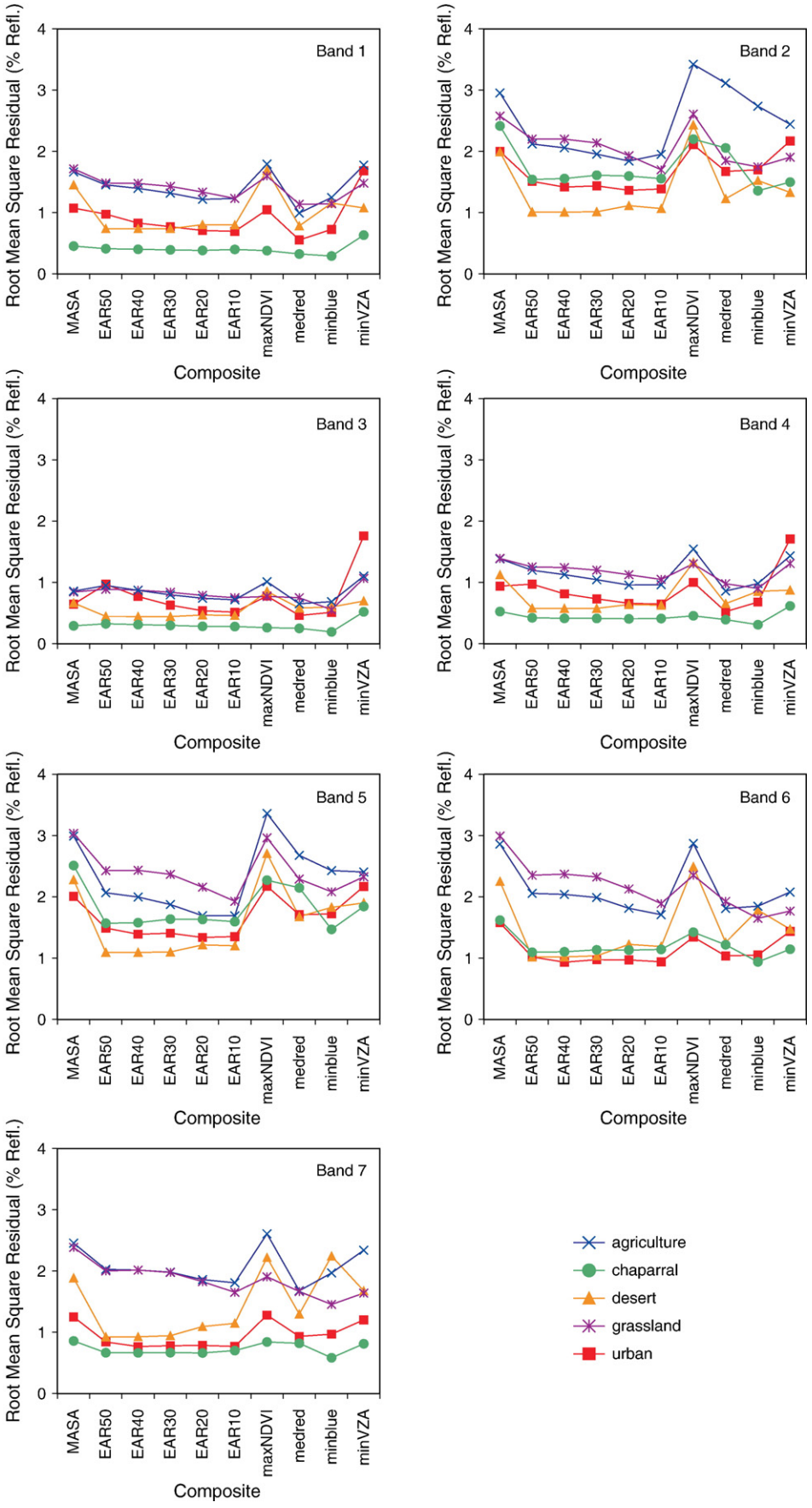

Fig. 7. The mean of root mean square residuals for each land cover type, for MODIS reflectance bands 1–7.

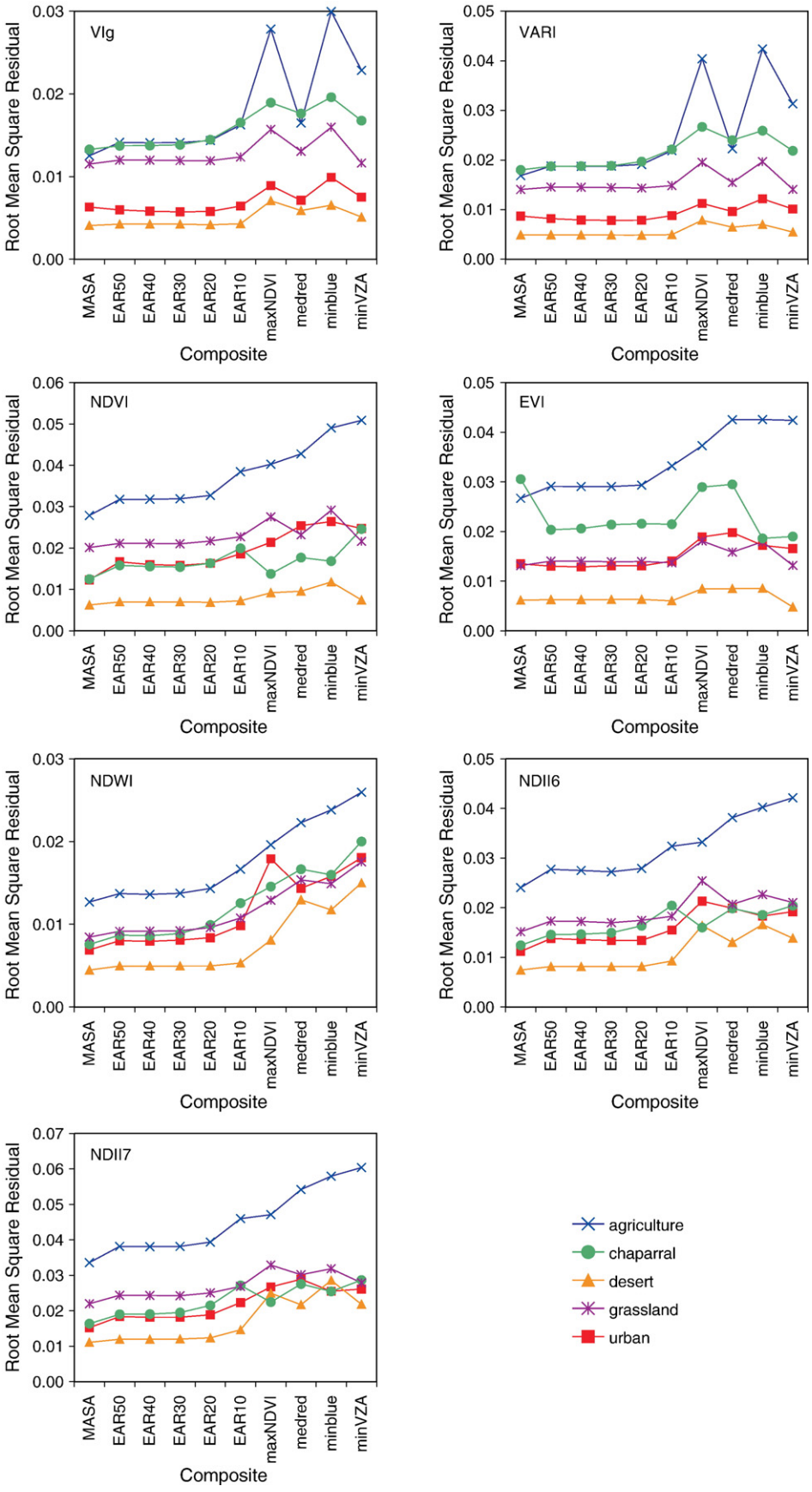

Fig. 8. The mean of root mean square residuals for each land cover type, for seven spectral indices.

Table 5
Mean r^2 values for comparisons of live fuel moisture and MODIS indices, averaged for 16 live fuel moisture samples at 11 sites

Composite	Index						
	VIg	VARI	NDVI	EVI	NDWI	NDII6	NDII7
MASA	*0.66*	*0.66*	*0.58*	0.45	*0.65*	*0.62*	*0.57*
EAR50	0.64	0.63	0.53	*0.53*	0.59	0.57	0.51
EAR40	0.64	0.64	0.54	0.52	0.59	0.57	0.52
EAR30	0.63	0.62	0.53	0.50	0.59	0.56	0.51
EAR20	0.61	0.61	0.50	0.44	0.51	0.55	0.50
EAR10	0.60	0.58	0.51	0.44	0.50	0.56	0.52
maxNDVI	0.56	0.55	0.45	0.30	0.55	0.55	0.48
medred	0.60	0.59	0.51	0.35	0.46	0.50	0.49
minblue	0.58	0.56	0.45	0.42	0.53	0.56	0.47
minVZA	0.58	0.57	0.44	0.50	0.37	0.55	0.47

The highest r^2 values for each composite is shown in italics.

are listed in order from least restrictive mean shade fraction constraint (EAR50) to most restrictive mean shade fraction constraint (EAR10). Residuals calculated for band values and residuals calculated for index values demonstrated contrasting trends. For band values, root mean square residuals were generally lowest for EAR10 or for one of the standard composites (Table 3). Overall root mean square residuals were lowest for visible bands 1, 3, and 4, due to lower reflectance caused by chlorophyll absorption in the visible spectrum. For these darker bands, the minred or minblue composites possessed the lowest root mean square residuals. For the brighter bands (2, 5, 6, and 7), the EAR10 composite possessed the lowest root mean square residuals. The maxNDVI and minVZA composites each produced the highest root mean square residuals for 3 out of the 7 bands. Comparing the shape-based composites, MASA and EAR algorithms most strongly favoring spectral shape had higher average residuals than EAR with more restrictive mean shade fraction constraints (Table 3).

In contrast to the residuals for band values, the root mean square residuals for six of the seven indices were lowest for the MASA composite (Table 4). The MASA composite possessed the lowest root mean square residual for every index except EVI. No single composite produced the highest residuals, with all four of the baseline composites possessing the highest root mean square residual for at least one band. The baseline composite residuals were uniformly higher than those from the MASA and EAR composites. Table 4 shows only two instances of a baseline composite with a lower root mean square residual than a MASA or EAR composite, both for EVI.

Plots of band root mean square residuals for each land cover type show that the agricultural and grassland land cover types consistently had the highest residuals (Fig. 7). Both land cover types also had higher variability in root mean square residuals when compared across the different compositing algorithms. The maxNDVI, minVZA, and MASA composites displayed the highest residuals across all five land cover types. The medred, minblue, and EAR10 composites generally produced the lowest residuals, although the desert root mean square residuals decreased as the mean shade fraction constraint was relaxed. Variations in the mean shade fraction constraint appeared to have little effect on residuals for chaparral.

Plots of index root mean square residuals for each land cover type show that the agricultural land cover type routinely had the highest residuals (Fig. 8). The desert land cover type had the lowest root mean square residuals, but this is at least partially due to the low index values associated with sparse vegetation cover. The MASA composite produced the lowest residuals for most indices across all five land cover types. A notable exception occurs for chaparral EVI, however. For chaparral EVI, the MASA composite had a higher root mean square residual than any of the other composites. In general, the EAR and MASA composites possessed lower residuals than the four baseline composites.

The lower variability of the MASA composite for most indices in the chaparral land cover type (Fig. 8) may translate to stronger correlations between indices and live fuel moisture. The MASA composite did produce higher average r^2 values than every other composite, for every index except EVI (Table 5). For EVI, the EAR50, EAR40, EAR30, and minVZA composites had higher average r^2 values than the MASA composite did. Over all composites, VARI and VIg had the strongest correlations with live fuel moisture. NDWI had lower average correlations than VIg and VARI for 3 of the 4 baseline compositing algorithms, but increased to nearly match the average r^2 values of VIg and VARI when the MASA or maxNDVI composites were used.

The significance of differences between composite correlation coefficients was tested for the seven indices for each of the 16

Table 6
The number of live fuel moisture samples (out of 16 possible) for which the pairing of the MASA composite and an index possessed a significantly higher r value (confidence level > 0.95) than the each composite listed and the same index

Composite	Index						
	VIg	VARI	NDVI	EVI	NDWI	NDII6	NDII7
EAR50	0	0	0	0	1	0	0
EAR40	0	0	0	0	2	0	0
EAR30	0	0	0	0	1	0	0
EAR20	0	0	1	0	3	0	0
EAR10	1	2	0	1	5	0	0
maxNDVI	5	5	5	5	4	2	3
medred	1	1	5	2	10	1	0
minblue	4	4	6	2	5	2	3
minVZA	3	3	6	0	15	2	2

Table 7
The number of live fuel moisture samples (out of 16 possible) for which a composite and index pairing possessed a significantly higher r value (confidence level > 0.95) than the MASA composite for the same index

Composite	Index						
	VIg	VARI	NDVI	EVI	NDWI	NDII6	NDII7
EAR50	0	0	0	2	0	0	0
EAR40	0	0	0	1	0	0	0
EAR30	0	0	0	0	0	0	0
EAR20	0	0	0	0	0	0	0
EAR10	0	0	0	0	0	0	0
maxNDVI	0	0	0	0	0	0	0
medred	0	0	0	0	0	0	0
minblue	0	0	0	1	0	0	0
minVZA	0	0	0	2	0	0	0

samples. Table 6 shows the number of samples, out of 16, for which the MASA composite had a significantly higher correlation compared with the each of the other composites. The differences between MASA and the baseline composite correlations were significant more often than the differences between MASA and other shape-based composite correlations. The largest number of significantly different correlations occurred for NDWI. Compared with minVZA, MASA was found to have significantly higher NDWI correlations for 15 sites, while compared with medred, MASA was found to have significantly higher NDWI correlations for 10 sites (Table 6). MASA also had several significantly higher correlations for NDVI. NDII6 and NDII7 had the smallest number of significantly different samples. Table 7 shows the number of samples, out of 16, for which at least one other composite had a significantly higher correlation than the MASA composite. EVI was the only index for which one of the other composites had significantly higher correlations for any samples. EAR50 and minVZA had significantly higher correlations than MASA for two samples, while EAR40 and minblue had significantly higher correlations for one sample.

5. Discussion

The MASA compositing algorithm produced the lowest index variability across nearly all land cover types and had the highest correlations with live fuel moisture. One of the few exceptions to this rule was for EVI. MASA produced higher EVI variability for the chaparral land cover type and had lower correlations with live fuel moisture compared with several of the EAR and baseline composites. These trends did not occur in any of the other land cover types, but it should be noted that chaparral has the highest leaf area index (LAI) of all of the land cover types tested. EVI was designed to reduce index sensitivity to atmospheric and soil background effects (Huete et al., 2002). It is possible that EVI's reduced sensitivity to these effects may negate any advantages that MASA confers through selection based entirely on spectral shape. Further analysis of MASA-based EVI for higher LAI land cover is needed.

NDWI was the index most improved by shape-based compositing. The highest root mean square residual for NDWI (minVZA) was more than twice the lowest root mean square residual (MASA), a greater difference than for any other spectral index. Shape-based composites produced improvements in NDWI residuals for all five land cover classes. NDWI also possessed the largest number of live fuel moisture samples for which MASA produced a significantly higher correlation. Unmasked cirrus clouds may be responsible for differences in NDWI variability and live fuel moisture correlations. NDWI is based on canopy water absorption at 1240 nm, but is also sensitive to absorption by cirrus (Gao, 1996). Examination of scatterplots of live fuel moisture versus NDWI calculated from the minVZA and medred composites showed several dates with anomalously high NDWI values, indicating increased water absorption. This increased water absorption is likely due to cirrus not flagged by MOD09GST. This anomaly is not present in the MASA composites, indicating that the shape-based compositing algorithms may have reduced sensitivity to cirrus contamination effects.

Correlations between live fuel moisture and spectral indices were highest for greenness indices based on green-to-red spectral contrast (VARI and VIg). These results agree with the findings of Stow et al. (2005) and Roberts et al. (2006). The differences between green/red index correlations and moisture index correlations are dependent on the compositing algorithm used, however. As compositing is increasingly weighted towards spectral shape, differences in the strengths of correlations narrow. For the MASA composite, average r^2 values for VARI, VIg, and NDWI are nearly identical.

While shape-based compositing algorithms may offer advantages over established algorithms, several important issues should be addressed before shape-based compositing can be used operationally. Shape-based metrics are dependent on the shapes of spectra within the compositing period class. Dissimilar spectral shapes introduced into the compositing period class may have a greater effect on MASA- and EAR-based compositing than on other compositing algorithms. For this reason, the effects of prescreening data on spectrum selection should be investigated. More research is needed to determine whether MASA can similarly reduce index variability across a variety of land cover types. MODIS images most of Earth's land surface daily, while this research analyzed composite variability within less than 0.05% of this land surface. Reduced variability and improvements in correlations produced by shape-based compositing may not extend to all vegetation measures. This research only analyzed ratio-based indices. Measures that use both spectral shape and brightness, such as SMA fractions, may have lower variability when calculated from an EAR composite rather than a MASA composite (Roberts et al., 2006). Shape-based algorithms are more computationally intensive than minimum or maximum value algorithms, so the practicality of using shape-based composites over larger areas should be investigated. The shape-based algorithms do not explicitly account for BRDF effects, and it is not known whether MASA or EAR favor particular view geometries. Finally, indices produced using different compositing algorithms should be compared to a wider variety of biophysical measures. Based on the reduction in index variability found by our research, it is likely that shape-based compositing algorithms will lead to improved correlations of indices with many vegetation properties.

6. Conclusions

The comparison of 10 different compositing algorithms demonstrates that there is no single "best" compositing algorithm possessing the lowest short-term variability. The compositing algorithms most dependent on spectral shape produced spectral indices with lower variability when compared with the baseline compositing methods. The MASA algorithm was shown to produce the lowest variability in six of the seven indices examined. However, shape-based compositing algorithms constrained to also take into account brightness, and baseline compositing algorithms, produced band brightness values with the lower variability compared with MASA. Further research on shape-based compositing algorithms is needed to investigate how these algorithms

reduce index variability, and to determine whether shape-based compositing algorithms can produce lower index variability across a wider variety of indices and land cover types. This future research may provide guidance for situations in which shape-based compositing should be favored over other compositing techniques.

Acknowledgements

Funding for this research was provided in part by a grant from the NASA Carbon Cycle Science program, award number NNG05GD12G, Mechanisms Controlling Annual, Interannual and Decadal Changes in California's Carbon Budget. MODIS data were obtained from the EROS Data Center. We thank Tom Bristow and J. Lopez of the Los Angeles County Fire Department, Forestry Division for supplying live fuel moisture data. We also thank the reviewers for their helpful comments.

References

Adams, J. B., Smith, M. O., & Gillespie, A. R. (1993). Imaging spectroscopy: Interpretation based on spectral mixture analysis. In C. M. Pieters & P. A. J. Englert (Eds.), *Remote geochemical analysis: Elemental and mineralogical composition* (pp. 145−166). Cambridge, England: Press Syndicate of University of Cambridge.

Ballantine, J. -A. C., Okin, G. S., Prentiss, D. E., & Roberts, D. A. (2005). Mapping African landforms using continental scale unmixing of MODIS imagery. *Remote Sensing of Environment*, *97*, 470−483.

Boardman, J. W., Kruse, F. A., & Green, R. O. (1995). *Mapping target signatures via partial unmixing of AVIRIS data in Summaries of the 5th JPL Airborne Earth Science Workshop. JPL Publication 95-1*, *Vol. 1* (pp. 23-26). Pasadena, CA: Jet Propulsion Laboratory.

Box, E. O., Holben, B. N., & Kalb, V. (1989). Accuracy of the AVHRR vegetation index as a predictor of biomass, primary productivity, and net CO_2 flux. *Vegetatio*, *80*, 71−89.

Cabral, A., De Vasconcelos, M. J. P., Pereira, J. M. C, Bartholome, E., & Mayaux, P. (2003). Multi-temporal compositing approaches for SPOT-4 VEGETATION. *International Journal of Remote Sensing*, *24*, 3343−3350.

Carreiras, J. M. B, & Pereira, J. M. C. (2005). SPOT-4 VEGETATION multi-temporal compositing for land cover change studies over tropical regions. *International Journal of Remote Sensing*, *26*, 1323−1346.

Carreiras, J. M. B., Pereira, J. M. C., Shimabukuro, Y. E., & Stroppiana, D. (2003). Evaluation of compositing algorithms over the Brazilian Amazon using SPOT-4 VEGETATION data. *International Journal of Remote Sensing*, *24*, 3427−3440.

Churkina, G., Schimel, D., Braswell, B. H., & Xiao, X. (2005). Spatial analysis of growing season length control over net ecosystem exchange. *Global Change Biology*, *11*, 1777−1787.

Chuvieco, E., Ventura, G., Martin, M. O., & Gomez, I. (2005). Assessment of multitemporal compositing techniques of MODIS and AVHRR images for burned land mapping. *Remote Sensing of Environment*, *94*, 450−462.

Cihlar, J., Manak, D., & D'Iorio, M. (1994). Evaluation of compositing algorithms for AVHRR over land. *IEEE Transactions on Geoscience and Remote Sensing*, *32*, 427−437.

Cihlar, J., Ly, H., Li, Z., Chen, J., Pokrant, H., & Huang, F. (1997). Multitemporal, multichannel AVHRR data sets for land biosphere studies — artifacts and corrections. *Remote Sensing of Environment*, *60*, 35−57.

Clark, R. N., & Roush, T. L. (1984). Reflectance spectroscopy: Quantitative analysis techniques for remote sensing applications. *Journal of Geophysical Research*, *89*, 6329−6340.

Countryman, C. M. & Dean, W. A. 1979. Measuring moisture content in living chaparral: A field user's manual. (Berkeley, CA: U.S. Dept. of Agriculture, Forest Service, Pacific Southwest Forest and Range Experiment Station).

Dennison, P. E., Halligan, K. Q., & Roberts, D. A. (2004). A comparison of error metrics and constraints for multiple endmember spectral mixture analysis and spectral angle mapper. *Remote Sensing of Environment*, *93*, 359−367.

Dennison, P. E., & Roberts, D. A. (2003). Endmember selection for multiple endmember spectral mixture analysis using Endmember Average RMSE. *Remote Sensing of Environment*, *87*, 123−135.

Dennison, P. E., & Roberts, D. A. (2003). The effects of vegetation phenology on endmember selection and species mapping in Southern California chaparral. *Remote Sensing of Environment*, *87*, 295−309.

Dennison, P. E., Roberts, D. A., Peterson, S. H., & Rechel, J. (2005). Use of normalized difference water index for monitoring live fuel moisture. *International Journal of Remote Sensing*, *26*, 1035−1042.

Duchemin, B., Guyon, D., & Lagouarde, J. P. (1999). Potential and limits of NOAA-AVHRR temporal composite data for phenology and water stress monitoring of temperate forest ecosystems. *International Journal of Remote Sensing*, *20*, 895−917.

Friedl, M. A., McIver, D. K., Hodges, J. C. F., Zhang, X. Y., Muchoney, D., Strahler, A. H., et al. (2002). Global land cover mapping from MODIS: Algorithms and early results. *Remote Sensing of Environment*, *83*, 287−302.

Gao, B. C. (1996). NDWI — a normalized difference water index for remote sensing of vegetation liquid water from space. *Remote Sensing of Environment*, *58*, 257−266.

Gitelson, A. A., Kaufman, Y., Stark, R., & Rundquist, D. (2002). Novel algorithms for remote estimation of vegetation fraction. *Remote Sensing of Environment*, *80*, 76−87.

Gutman, G. G., Ignatov, A. M., & Olson, S. (1994). Towards better quality of AVHRR composite images over land: Reduction of cloud contamination. *Remote Sensing of Environment*, *50*, 134−148.

Harsanyi, J. C., & Chang, C. I. (1994). Hyperspectral image classification and dimensionality reduction: An orthogonal subspace projection approach. *IEEE Transactions on Geoscience and Remote Sensing*, *32*, 779−785.

Holben, B. N. (1986). Characteristics of maximum value composite images from temporal AVHRR data. *International Journal of Remote Sensing*, *7*, 1417−1434.

Huete, A. R., Didan, K., Miura, T., Rodriguez, E. P., Gao, X., & Fereira, L. G. (2002). Overview of the radiometric and biophysical performance of the MODIS vegetation indices. *Remote Sensing of Environment*, *83*(1–2), 195−213.

Hunt, R. E., & Rock, B. N. (1989). Detection of changes in leaf water content using near- and middle-infrared reflectances. *Remote Sensing of Environment*, *30*, 43−54.

Kasischke, E. S., & French, N. H. F. (1997). Constraints on using AVHRR composite index imagery to study patterns of vegetation cover in boreal forests. *International Journal of Remote Sensing*, *18*, 2403−2426.

Kruse, F. A., Lefkoff, A. B., Boardman, J. W., Heidebrecht, K. B., Shapiro, A. T., Barloon, P. J., et al. (1993). The Spectral Image-Processing System (SIPS) — interactive visualization and analysis of imaging spectrometer data. *Remote Sensing of Environment*, *44*, 145−163.

LACFD (Los Angeles County Fire Department, Forestry Division) 2000, 2001, 2002, 2003, 2004, 2005 Live fuel moisture summary, http://www.lacofd.org/Forestry_folder/Life_Fuel_Moisture.htm

Loveland, T. R., Reed, B. C., Brown, J. F., Ohlen, D. O., Zhu, Z., Yang, L., et al. (2000). Development of a global land cover characteristics database and IGBP DISCover from 1 km AVHRR data. *International Journal of Remote Sensing*, *21*, 1303−1330.

Lunetta, R. L., Knight, F. K., Ediriwickrema, J., Lyon, J. G., & Worthy, L. D. (2006). Land-cover change detection using multi-temporal MODIS NDVI data. *Remote Sensing of Environment*, *105*, 142−154.

Papoulis, A. (1990). *Probability and statistics.* Englewood Cliffs, NJ: Prentice Hall.

Paruelo, J. M., & Lauenroth, W. K. (1998). Interannual variability of NDVI and its relationship to climate for North American shrublands and grasslands. *Journal of Biogeography*, *25*, 721−733.

Powell, R. L., Roberts, D. A., Dennison, P. E., & Hess, L. L. (2007). Sub-pixel mapping of urban land cover using multiple endmember spectral mixture analysis: Manaus, Brazil. *Remote Sensing of Environment*, *106*, 253−267.

Qi, J., & Kerr, Y. (1997). On current compositing algorithms. *Remote Sensing Reviews*, *15*, 235−256.

Roberts, D. A., Dennison, P. E., Peterson, S., Sweeney, S., & Rechel, J. (2006). Evaluation of AVIRIS and MODIS measures of live fuel moisture and fuel

condition in a shrubland ecosystem in southern California. *Journal of Geophysical Research — Biogeosciences*, *111*, G04S02.

Roberts, D. A., Gardner, M., Church, R., Ustin, S., Scheer, G., & Green, R. O. (1998). Mapping chaparral in the Santa Monica Mountains using multiple endmember spectral mixture models. *Remote Sensing of Environment*, *65*, 267−279.

Rouse, J. W., Haas, R. H., Schell, J. A., & Deering, D. W. (1973). Monitoring vegetation systems in the Great Plains with ERTS. Third ERTS Symposium. *NASA SP351*, *Vol. 1* (pp. 309-317).

Roy, D. P. (1997). Investigation of the maximum normalized difference vegetation index (NDVI) and the maximum surface temperature (T_s) AVHRR compositing procedures for the extraction of NDVI and T_s over forest. *International Journal of Remote Sensing*, *18*, 2383−2401.

Roy, D. P., Borak, J. S., Devadiga, S., Wolfe, R. E., Zheng, M., & Descloitres, J. (2002). The MODIS land product quality assessment approach. *Remote Sensing of Environment*, *83*, 62−76.

Schaaf, C. B., Gao, F., Strahler, A. H., Lucht, W., Li, X., Tsang, T., et al. (2002). First operational BRDF, albedo and nadir reflectance products from MODIS. *Remote Sensing of Environment*, *83*, 135−148.

Stow, D., Niphadkar, M., & Kaiser, J. (2005). MODIS-derived visible atmospherically resistant index for monitoring chaparral moisture content. *International Journal of Remote Sensing*, *26*, 3867−3873.

van Leeuwen, W. J. D., Huete, A. R., & Laing, T. W. (1999). MODIS vegetation index compositing approach: A prototype with AVHRR data. *Remote Sensing of Environment*, *69*, 264−280.

Vermote, E. F., El Saleous, N. Z., & Justice, C. O. (2002). Atmospheric correction of MODIS data in the visible to middle infrared: First results. *Remote Sensing of Environment*, *83*, 97−111.

Vermote, E. F., El Saleous, N. Z., Justice, C. O., Kaufman, Y. J., Privette, J. L., Remer, L., et al. (1997). Atmospheric correction of visible to middle-infrared EOS-MODIS data over land surfaces: background, operational algorithm and validation. *Journal of Geophysical Research — Atmosphere*, *102*(D14), 17131−17141.

Vermote, E. F., & Vermeulen, A. (1999). *Atmospheric correction algorithm: Spectral reflectances (MOD09).* MODIS algorithm theoretical basis document.

Weise, D. R., Hartfor, R. A., & Mahaffey, L. (1998). Assessing live fuel moisture for fire management applications. Fire in ecosystem management: shifting the paradigm from suppression to prescription. In T. L. Pruden & L.A. Brennan (Eds.), *Tall Timbers Fire Ecology Conference Proceedings*, *Vol. 20* (pp. 49-55). Tallahassee, FL: Tall Timbers Research Station.

Wolfe, R. E., Roy, D. P., & Vermote, E. F. (1998). The MODIS land data storage, gridding and compositing methodology: LEVEL 2 Grid. *IEEE Transactions on Geoscience and Remote Sensing*, *36*, 1324−1338.